HAYATI
Journal of Biosciences

Vol. 30 No. 6, November 2023 1025-1035
DOI:10.4308/hjb.30.6.1025-1035
ISSN: 1978-3019
EISSN: 2086-4094

Molecular Docking and Dynamics of SARS-CoV-2 Programmed Ribosomal Frameshifting RNA and Ligands for RNA-Targeting Alkaloids Prospecting

Adhityo Wicaksono[1], Arli Aditya Parikesit[2*]

[1]Division of Biotechnology, Genbinesia Foundation, Gresik 61171, Indonesia
[2]Department of Bioinformatics, School of Life Sciences, Indonesia International Institute of Life Sciences, East Jakarta 13210, Jakarta Capital Region, Indonesia

ARTICLE INFO

Article history:
Received September 19, 2022
Received in revised form June 16, 2023
Accepted June 23, 2023

KEYWORDS:
Bioactive compound,
computer-assisted drug design,
computational biology,
intercalating agent,
nucleic acid docking,
plant metabolites

ABSTRACT

RNA-ligand docking is a part of computational biology, which is currently lowly recognized compared to the protein-ligand docking procedure commonly applied for drug discovery. This *in silico* study aims to create a simplified protocol for RNA-ligand docking, which is applicable to RNA-targeting small molecular drug screening. Four alkaloids (berberine, colchicine, nicotine, and tomatine) were subjected to this study and contended against the SARS-CoV-2 genomic RNA -1 PRF component targeting control drug, merafloxacin, including two known intercalator berberine and colchicine, a small alkaloid nicotine and a large alkaloid tomatine. The alkaloids were screened for drug-likeness properties (Lipinski's Rules of 5 or LRo5), bioavailability indexes, and synthetic accessibility values using SwissADME before docking. The docking used PyRx – Autodock Vina and re-scored for RNA-ligand scoring using AnnapuRNA. The docking results have the interactions mapped using fingeRNAt and visualized using Discovery Studio. Molecular dynamics using CHARMM36 and AMBER forcefields were simulated in NAMD. The molecular dynamics 1 ns simulation results showed that the ligand interaction over time did not cause much interference with the RNA, indicated by the low number of RMSD changes between RNA itself and the RNA-ligand complex. Additionally, CHARMM36 forcefield provided more stable fluctuation compared to AMBER. The results indicated that tomatine disobeyed LRo5 and had a low bioavailability index and bad synthetic accessibility value, while the rest alkaloids passed. In the end, berberine has an even higher docking score than the control drug. The study also shows that this protocol can be useful for future RNA-ligand computational studies.

1. Introduction

Ribonucleic acid (RNA) serves as structural and functional macromolecules of a biological organism. Virus, for instance, uses RNA as their main genetic storage and blueprint molecules, specifically for viruses classified under class III, IV, V and VI of the Baltimore classification system (Baltimore 1971). The RNA viruses transfer their genomic RNA to the host cells, where the genetic information is later translated to virus-constructing proteins using the host ribosomes or replicated to produce more viral RNA using RNA-dependent RNA polymerase (RdRP) (Koonin *et al.* 1989). Fascinatingly, the programmed ribosomal frameshifting (PRF) component is an RNA component commonly found in viruses that allows the ribosome to slip during translation by specific amounts of nucleobases forward or backward, causing the diversity of the translated viral proteins by codon reading frameshift (Atkins *et al.* 2016). The PRF comprises a frameshift element (FE) with slippery-inducing structures that induce the frameshift, either by ribosomal interacting signal elements or mRNA interacting trans-acting elements (Napthine *et al.* 2017). Typically, the frameshift is by 1 nucleotide backward (hence, -1 PRF) (e.g., in coronaviruses) (Kelly *et al.* 2020). Rarely, there are also 1 nucleotide forwards (+1

* Corresponding Author
E-mail Address: arli.parikesit@i3l.ac.id

PRF) (e.g., in *Escherichia coli* and *Saccharomyces cerevisiae*) (Craigen and Caskey 1986; Dinman 2012) and 2 nucleotides backward (-2 PRF) (e.g., in Arteriviridae order Nidovirales) (Snijder *et al.* 2013; Napthine *et al.* 2016). These RNA structural and functional versatility are not only limited by virus-bound RNA but there are more, e.g., RNA cleaving hammerhead ribozyme (Stage-Zimmermann and Uhlenbeck 1998), plant viroid (Ding and Itaya 2007), to gene silencing microRNA or miRNA (Jonas and Izaurralde 2015).

To control viral infection, drugs are classified to their specific mechanisms. Many drugs are used to target and inhibit the viral protein. For instance, some drugs target the RNA-replicating RdRP enzyme, e.g., molnupiravir (Hashemian *et al.* 2022) and remdesivir (Zhang and Zhou 2020) that block RdRP in severe acute respiratory syndrome coronavirus 2 (SARS-CoV2). The other drugs target the surface protein, like oseltamivir which inhibits neuraminidase in the influenza A virus (McNicholl and McNicholl 2001). The rest of many drugs target the other viral functional proteins that play roles in viral structural assembly (Saxena 2020). There is only a very limited type of drug or drug candidates which are targeting the viral RNA to inhibit the RNA-specific processes. The example is merafloxacin, originally an antibacterial drug, which could block the RNA pseudoknot formation in the PRF component (Sun *et al.* 2021). Supposedly, there should be more drugs out there that possess this ability, thus adding more to the drug diversity. Screening for drug candidates by computer-assisted method will be an important step to make the process more efficient. However, the computer-assisted drug design (CADD) and screening process, e.g., molecular docking and molecular dynamics, are mainly performed on protein/enzyme-inhibiting drug candidates. The study CADD to screen the potential RNA-targeting drug candidates using molecular docking of RNA receptors is still limited, despite the number of potential drugs and natural, biological origin metabolite compounds to screen.

This study is focused on molecular docking and dynamics of viral -1 PRF RNA, which serves as an example of how the RNA-targeting drug screening working pipeline could be done. The alkaloids were specifically chosen for this study as the drug candidates because some are already characterized as potential DNA intercalating agents and thus assumed to also interfere with RNA structure. Despite the reductionist concept of this study, just like the CADD in protein-targeting drugs, the work results could serve as the preliminary methods that later will be optimized by more *in vitro* bioassays, including the optimization to improve the drug delivery to the target RNA system.

2. Materials and Methods

2.1. RNA and Alkaloids *In Silico* Preparations

The RNA macromolecule used in the study is a 29-kDA frameshift element motif located at the ORF1a 3' end of the SARS-CoV-2 RNA sequence of -1 PRF, composed of 88 nucleotides (PDB ID: 6XRZ) (Figure 1A and Table 1) (Zhang *et al.* 2021). To set the RNA into macromolecule receptor in Autodock Vina (on PyRx v0.8), the PDB file of the RNA was converted with Open Babel v2.3.1 (O'Boyle *et al.* 2011) to the PDBQT format. The control ligands and the subjected alkaloids ligands were obtained from Human Metabolome Database (HMDB) (https://hmdb.ca) in three-dimensional PDB format. The control, merafloxacin (HMDB0254459) (Figure 1B), was contended against the intercalator alkaloids (Abookleesh *et al.* 2022), berberine (HMDB0003409) (Figure 1C) and colchicine (HMDB0015466) (Figure 1D). Additionally, two alkaloids that with unknown intercalating ability consisted of a small alkaloid, nicotine (HMDB0001934) (Figure 1E) and large alkaloid, tomatine (HMDB0034103) (Figure 1F) were also tested for docking. The details, including SMILES codes of each molecule, are available in Table A.1. All alkaloids were submitted to SwissADME (http://www.swissadme.ch/index.php) (Daina *et al.* 2017) to obtain the molecular weight, drug-likeness of Lipinski's Rules of 5 (LRo5), bioavailability and synthetic accessibility.

2.2. Molecular Docking and Observation of Molecular Interaction

To perform molecular docking, an RNA-ligand docking protocol using Autodock Vina and validated by AnnapuRNA was used (Stefaniak and Bujnicki 2021). Autodock Vina (Trott and Olson 2009) in PyRx v0.8 selective docking procedure was chosen on the space centered surrounding the slippery sequence of -1 PRF (X: 87.68, Y: 77.49 and Y: 58.53) with Vina search space dimension of 25 Å on all X, Y, and Z axes. After docking, the docked

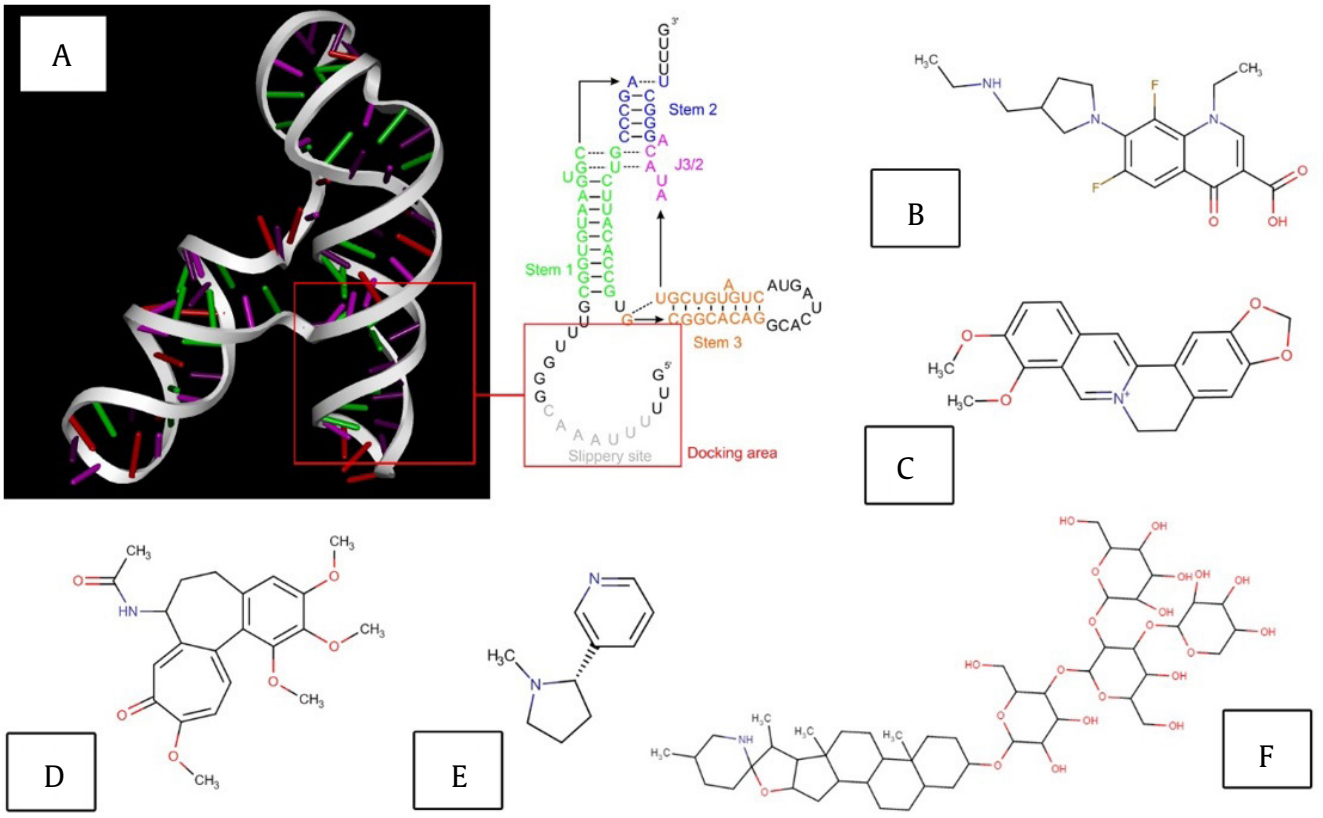

Figure 1. Elements of this *in silico* experiment: 88 nucleotides long frameshift element component of -1 PRF in SARS-CoV-2 RNA genome with the schematics and docking area (A), the control drug merafloxacin (B) and the alkaloids, consist of berberine (C), colchicine (D), nicotine (E) and tomatine (F)

Table 1. Chemical properties, drug-likeness on Lipinski's Rules of 5 (LRo5), bioavailability and synthetic accessibilities acquired using SwissADME

Metabolites	Plant source	Average molecular weight (g/mol)	Obey lipinski rule of five?	Bioavailability score	Synthetic accessibility
Merafloxacin	-	379.4	Yes (0)	0.55	3.33
Berberine	*Berberis vulgaris* L.	336.361	Yes (0)	0.55	3.14
Colchicine	*Colchicum autumnale* L.	399.437	Yes (0)	0.55	3.87
Nicotine	*Nicotiana tabacum* L.	162.232	Yes (0)	0.55	2.05
Tomatine	*Solanum lycopersicum* L.	1034.188	No (3)	0.17	10.00

ligand with new docked coordinates was saved in PDB format from PyRx and converted to SDF format using Discovery Studio 2021 (Dassani Systems). RNA-ligand interaction sites were analyzed using fingeRNAt (Szulc *et al.* 2022). A three-dimensional general view and bonds contributing nucleotides of the docked system were visualized using Discovery Studio 2021 (Dassani Systems). Both AnnapuRNA and fingeRNAt were executed under Windows Subsystem for Linux (WSL) Ubuntu v20.04.4 LTS (GNU/Linux 4.4.0-22000 Microsoft x86_64).

2.3. Molecular Dynamics

The molecular dynamics were tested under two different forcefields known to support RNA, and the docked systems were solvated and had the forcefield set using CHARMM-GUI online server (https://charmm-gui.org) (Lee *et al.* 2016). The first one is CHARMM36 forcefield, an optimized version of CHARMM27 forcefield (Hart *et al.* 2012; Xu *et al.* 2016). The second one is AMBER forcefield, with OL3 and GAFF parameters set for RNA and ligand, respectively. AMBER OL3 parameter is the most

suitable RNA forcefield (Zgarbová *et al.* 2011). These two forcefield settings were used to select the most stable forcefield for RNA-ligand systems. Typically, to measure the total energy within the forcefield (U), bond stretch (K_b is the force constant, while $b–b_0$ is the change in bond distance), angle changes (K_θ is the force constant, while $\theta–\theta_0$ is the atomic angular change) and dihedral torsion (K_x is the force constant, n refers to diversity, and $\varphi–\varphi_0$ is the torsional change) are counted for intramolecular energy. In contrast, van der Waals non-charged molecular interactions (ε for the potential energy, R for atomic radius, r for interatomic distance, while i and j represent two different molecules) and Coulomb electrostatic energy (q for molecular charges, ε_0 for electric constant, r for intermolecular distance, while i and j representing two different molecules) are measured for intermolecular energy. These calculations were used in the forcefield settings of OPLS (Jorgensen *et al.* 1996) and AMBER (Cornell *et al.* 1995), see Eq. 1. However, the CHARMM forcefield settings added improper torsion (K_Φ is the force constant, while $\Phi–\Phi_0$ is the out-of-plane angle) calculations, which is similar to GROMOS forcefield (Petrov *et al.* 2013) and Urey-Bradley potentials (K_{UB} is the force constant, while $S–S_0$ is the change of the distance of non-bonded atoms of the same molecule, or 1-3 bonded atom), see Eq. 2 or simplified to Eq 3.

$$U_{AMBER}(\mathrm{r}) = \sum_{bonds} K_b (b - b_0)^2 + \sum_{angles} K_\theta (\theta-\theta_0)^2 + \sum_{dihedrals} K_x (1 + \cos(n\varphi - \varphi_0)) + \sum_{non\text{-}bonded} \left(\varepsilon_{ij} \left[\left(\frac{R_{min,ij}}{r_{ij}} \right)^{12} - 2 \left(\frac{R_{min,ij}}{r_{ij}} \right)^{6} - 2 \right] + \frac{q_i q_j}{4\pi\varepsilon_0 r_{ij}} \right) \quad (1)$$

$$U_{CHARMM}(\mathrm{r}) = \sum_{bonds} K_b (b - b_0)^2 + \sum_{angles} K_\theta (\theta - \theta_0)^2 + \sum_{dihedrals} K_x (1 + \cos(n\varphi - \varphi)) + \sum_{Urey\text{-}Bradley} K_{UB} (S - S_0)^2 + \sum_{impropers} K_\phi (\phi - \phi_0)^2 + \sum_{non\text{-}bonded} \left(\varepsilon_{ij} \left[\frac{R_{min,ij}}{r_{ij}} \right)^{12} - 2 \left(\frac{R_{min,ij}}{r_{ij}} \right)^{6} \right] + \frac{q_i q_j}{4\pi\varepsilon_0 r_{ij}} \quad (2)$$

$$U_{CHARMM}(r) = U_{AMBER}(r) + \sum_{\text{Urey-Bradley}} \mathrm{K_{UB}} (S - S_0)^2 + \sum_{impropers} K\phi (\phi - \phi_0)^2 \quad (3)$$

The separated docked systems (RNA receptor and ligands, in PDB format) were merged using PyMol v2.5.1 (Schrodinger LLC). PDB complex preparation with CHARMM-GUI (two different forcefield types: CHARMM36 and AMBER, octahedral water box with NaCl ion added with Monte-Carlo placement method for charge neutralization, NPT ensemble, and default ambient temperature of 303.15 K) for Nanoscale Molecular Dynamics (NAMD) input. Using the output of CHARMM-GUI, the molecular dynamics were performed using NAMD v2.1.4 (Phillips *et al.* 2005) (operated using Windows PowerShell) for 1 ns. Visualization of complex root-mean-squared deviation (RMSD) and hydrogen bonds in Visual Molecular Dynamics (VMD) v1.9.4 (Humphrey *et al.* 1996).

3. Results

3.1. Alkaloid Ligands Chemical and Drug-Likeness Properties

Screened using SwissADME, it appears that almost all of the alkaloids, even including the control drug (merafloxacin), obey LRo5, possessing tolerable bioavailability values (almost entirely 0.55) and synthetic accessibility values (almost all less than 3.5) except for tomatine (Table 1). Tomatine has a very high molecular weight compared to the rest (1034.188 g/mol), very low bioavailability (0.17) and synthetic accessibility at the end of the hardness spectrum (10). Additionally, tomatine deviates from LRo5 as its molecular weight is higher than 500 g/mol, hydrogen acceptors are more than 10 and hydrogen donors are more than 5. Making it possesses low quality of drug-likeness properties. All the known intercalators, berberine and colchicine, and even the small alkaloid nicotine, have properties that are acceptable for drug-likeness that is similar to merafloxacin.

3.2. Interactions of -1 PRF RNA and Alkaloid Ligands

The alkaloids were docked on different positions of the same site (slippery site near the 5' end of the RNA) on the RNA band (Figure 2). The control drugs merafloxacin, berberine and tomatine are docked between the loop, consisting of a strand of 5' terminus with the strand with the slippery site sequence (see Figure 2A, B, and E). Distinctively, colchicine and nicotine interact more externally (not between the strand but instead, located farther away probably interacting with more sequences in the nearby strand; see Figure 2C and D). Scored using AnnapuRNA, the top three docked molecules are tomatine, berberine, and merafloxacin, in order from the most negative to the more positive docking scores of the three (Table 2; see total docking scores). Judging from the total number of bonds detected by fingeRNAt (Table 2; see total bonds), the top three are tomatine, merafloxacin,

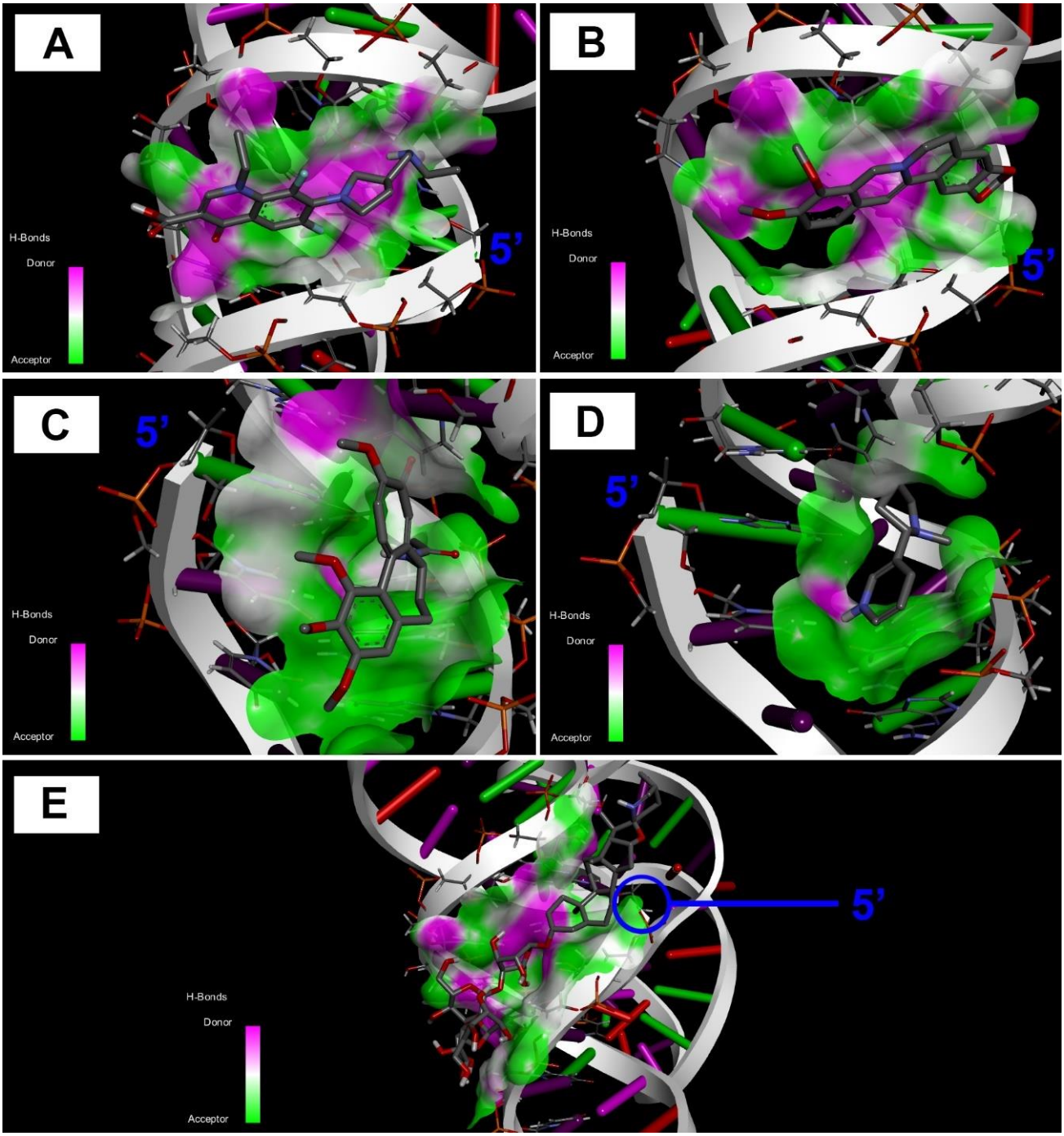

Figure 2. The RNA-alkaloid ligand docking complexes, revealing the variations of ligand positions in the slippery site of the -1 PRF RNA (in 5' terminus, indicated in blue; referring to the schematics in Figure 1A). Ligands: merafloxacin–the control drug (A), berberine (B), colchicine (C), nicotine (D) and tomatine (E)

and colchicine, in order from the highest to the lowest of the three. Nicotine is the most consistent in term of the weakest for the docking scores and total bonds formed during docking. However, like nicotine, berberine has the lowest bond values, but berberine has the second strongest docking score that even surpassed the control drug, merafloxacin.

3.3. Molecular Dynamics

The result of molecular dynamics simulations revealed distinctive characteristics of the RMSD graphs for both CHARMM36 forcefield and AMBER forcefield (Figure 3; Table A.2 for CHARMM36; Table A.3 for AMBER). However, there were problems with tomatine before and after the simulation. In the pre-

Table 2. Docking scores of RNA-alkaloid complexes and the bond-contributing nucleotides of the RNA chain

Metabolites	Total docking score (kcal/mol)	Hydrogen bonds-contributing nucleotides	Lipophilic bonds-contributing nucleotides	Other bonds-contributing nucleotides	Total bonds
Merafloxacin	-143.764	0, 2, 12, 13, 15, 16	2, 16	1 (Halogen)	9
Berberine	-157.078	16	2, 16	-	3
Colchicine	-64.043	0, 12, 45	0, 1, 12, 45	-	7
Nicotine	-74.402	1, 12	12, 45	-	3
Tomatine	-371.454	0, 1, 2, 3, 12, 13, 14	0, 1, 2, 3, 13, 14, 16	-	14

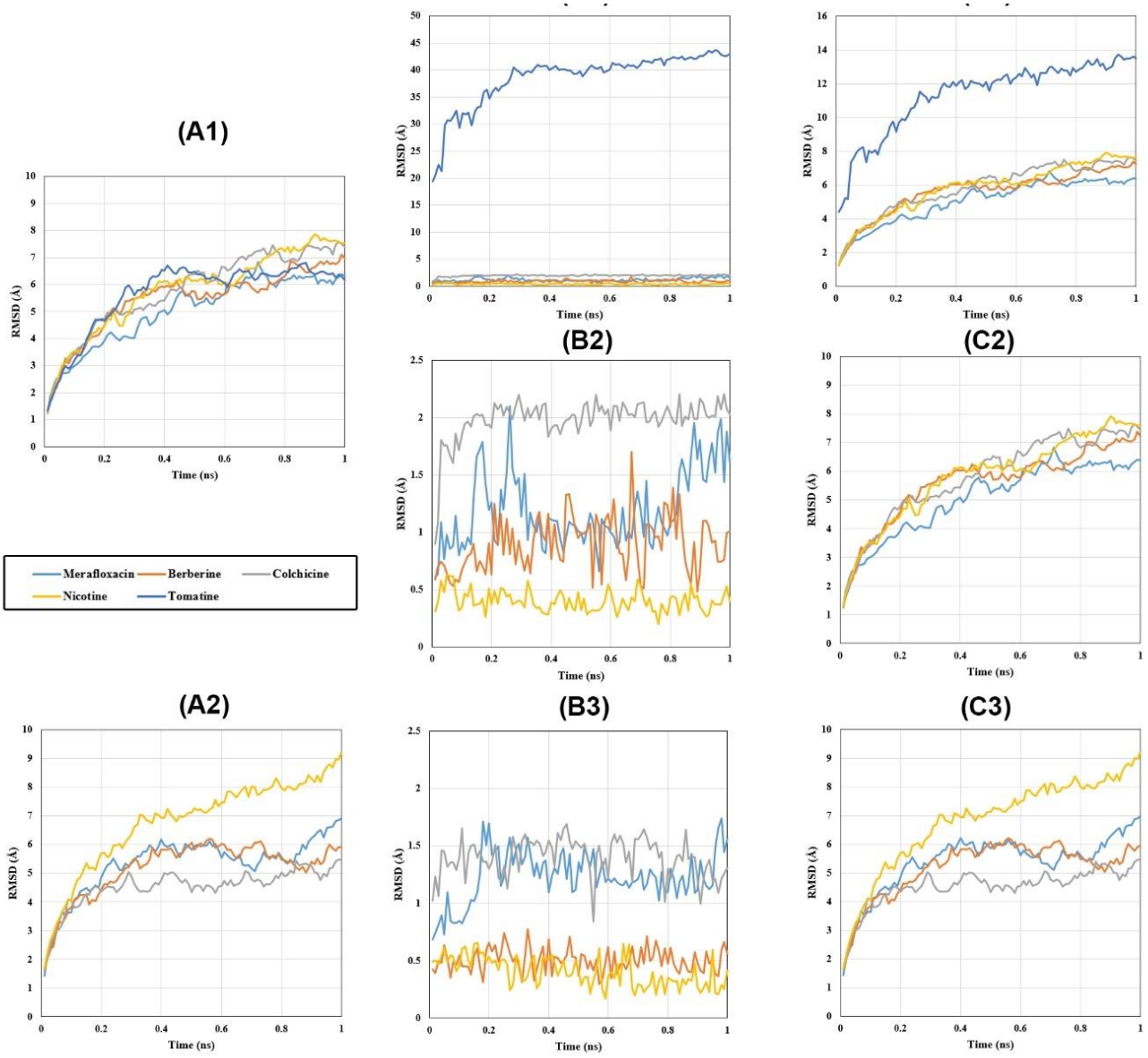

Figure 3. Molecular dynamics of RNA (on each simulation with the specified ligand), ligands, and RNA-ligand complex, showing the differences in root-mean-squared deviation (RMSD) pattern per time of simulation (1 ns of simulation run): The RNA in CHARMM36 forcefield (A1) and AMBER forcefield (A2). The ligands (all 5) in CHARMM36 (B1), show the great fluctuation in tomatine indicated by high RMSD values. The ligands (excluding tomatine) in CHARMM36 (B2) and AMBER (B3). The RNA-ligands in CHARMM36 for all 5 complexes (C1), excluding tomatine in CHARMM36 (C2) and in AMBER (C3). The RNA-tomatine complex was unable to be processed in CHARMM-GUI for AMBER forcefield

simulation problem, the RNA-tomatine complex was unable to be processed in CHARM-GUI for AMBER forcefield preparation for molecular dynamics, as the tomatine was identified as glycan molecule but later, the structure was unprocessable as the molecules is detected as modified glycan and causing error. Hence tomatine was excluded on AMBER simulation. The post-simulation problem is, tomatine is highly fluctuating as the ligand itself (Figure 3B1) and even as a complex with RNA (Figure 3C1). It is hard to observe and compare with the rest of the alkaloids. Therefore, in many results, tomatine-excluded graphics for CHARMM36 simulation are also provided (Figure 3B2 and C2).

The RMSD shown in CHARMM36 forcefield simulation results appear to be more consistent and less fluctuating for all subjected ligands, compared to AMBER (OL3 parameter) results especially after the climbing stage (prior to 0.4 ns) ends (Figure 3A1 and A2 for CHARMM36 and AMBER, respectively). The period of 0.4 ns is marked as the end of climbing stage as the RMSD curves appear to be more consistent and fluctuating in less steeper surges toward the end of the simulation (1 ns). However, the alkaloid ligands appear to be an orderly and stable fluctuation of RMSD when simulated in AMBER (GAFF parameter) compared to CHARMM36 (Fig. 3B2 and B3 for CHARMM36 and AMBER, respectively). In the RNA-alkaloid complexes, the graphs shown from CHARMM36 (Figure 3C2) are more consistent than those from AMBER (Figure 3C3), which are slightly diverged. Indicating more stable fluctuation in the CHARMM36 simulation.

From an overall perspective, the graph of plain RNA simulation (Figure 3A1-2) versus RNA-alkaloid complexes (Figure 3C2-3) appear just identical unless looking at the data values by themselves (see Table A.2 and Table A3) or measuring the RMSD differences (ΔRMSD). The RMSD differences between plain RNA and RNA-ligand complexes reveal the details between CHARMM36 and AMBER forcefield simulation of molecular dynamics (Figure 4; Table A.4). Once again, tomatine shows a massive difference of RMSD in CHARMM36 simulation compared to the other specimen ligands (Figure 4A), which zoomed out the other ligand results. By removing tomatine, the differences in other alkaloids under CHARMM36 forcefield can be seen (Figure 4B). Although the difference of RMSD in nicotine appears to be higher, the simulations in CHARMM36 forcefield appear to be relatively stable compared to AMBER (Figure 4C), which reveals many negative results (the RNA-ligand complex is less fluctuating than RNA by itself). In CHARMM36 ΔRMSD graphic, there are few negative values, but they are not higher than -0.02 Å (less than halfway to -0.05 Å). As for the hydrogen bond graphs (Figure 5; tomatine excluded), all RNA-alkaloid hydrogen bonds are not higher than 1, rarely reaching the optimum of 2 bonds. However, no bond is detected in the AMBER forcefield result on nicotine.

Comparable to molecular docking results, which point to berberine versus colchicine, both showed to have a stable fluctuation of RMSD as seen in both RNA-ligand complexes of CHARMM36 and AMBER forcefields (Figure 3C2 and C3). Although

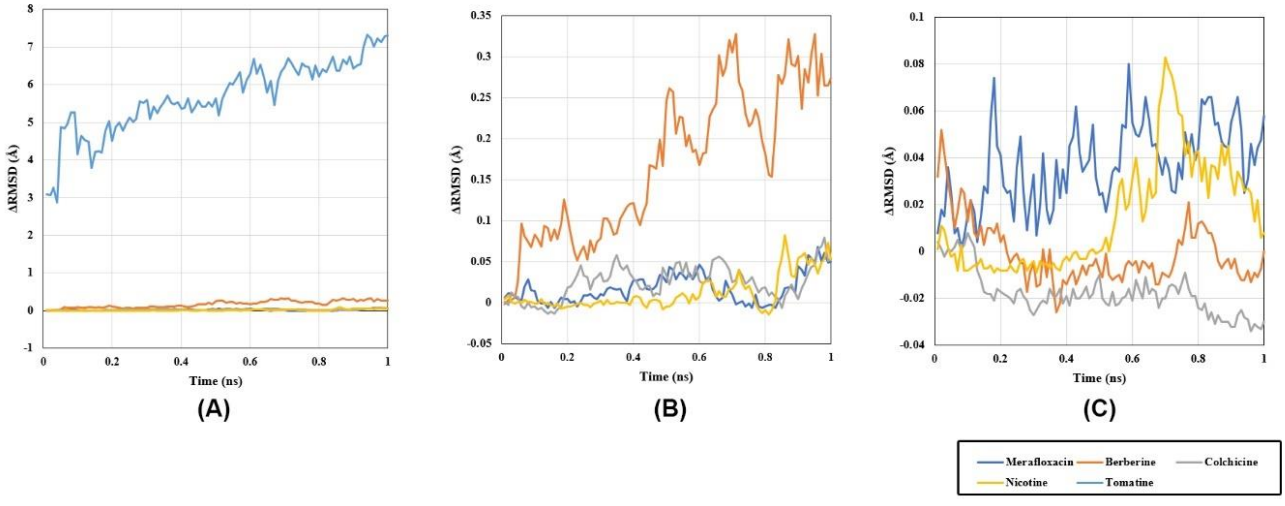

Figure 4. Differences of RMSD value between RNA-ligand complexes and RNA-only simulations reveal the complexes' fluctuation and distinctive features by CHARMM36 (A-B) and AMBER (C) forcefields. Tomatine possesses high RMSD differences (A) under CHARMM36, while the rest of the complexes have differences of less than 0.5, for both CHARMM36 (B) and AMBER (C) by excluding tomatine from the graphs

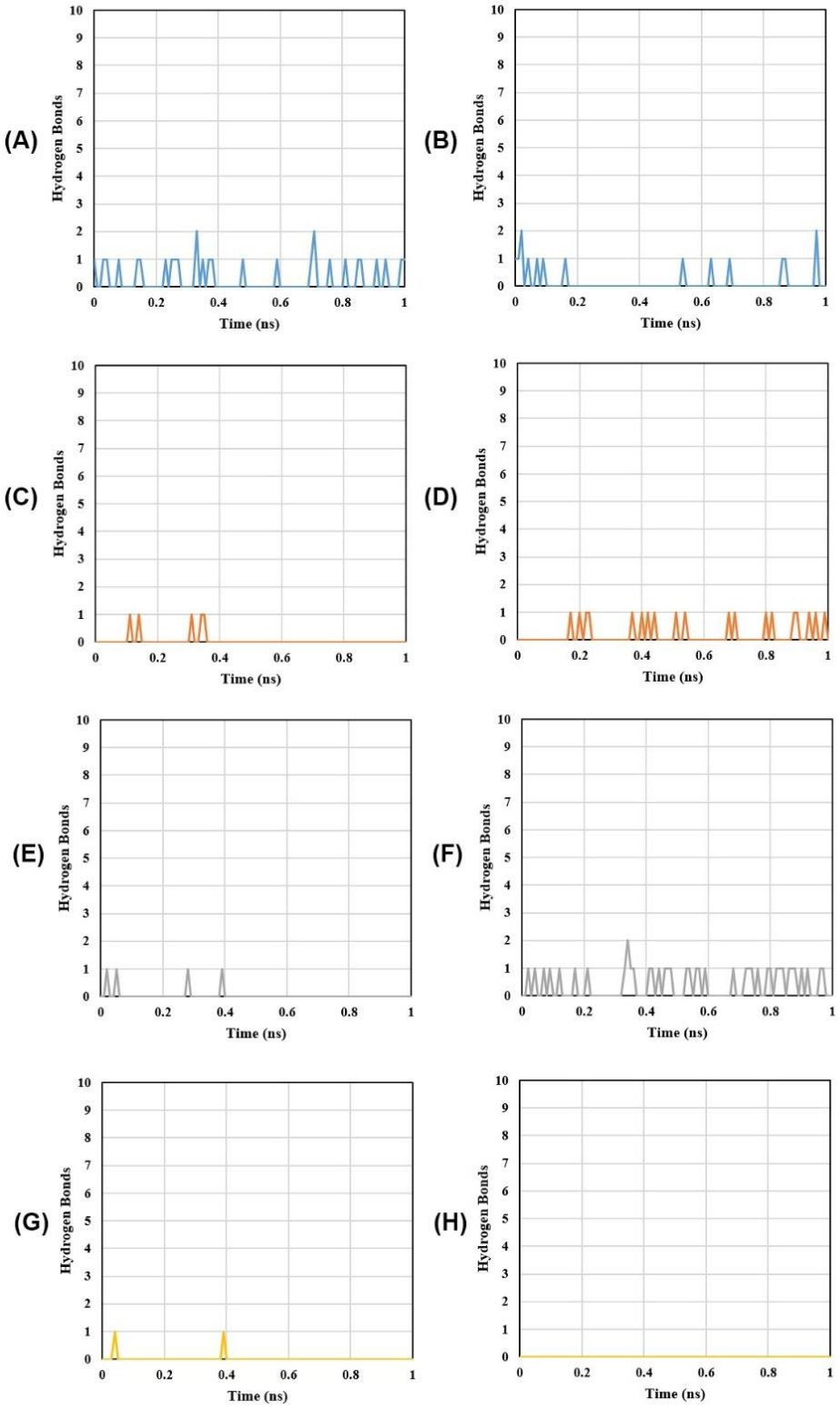

Figure 5. Fluctuations in RNA-ligand complex hydrogen bond values per time of the simulation. Complex of RNA with merafloxacin in CHARMM36 (A) and AMBER (B), berberine in CHARMM36 (C) and AMBER (D), colchicine in CHARMM36 (E) and AMBER (F), and nicotine in CHARMM36 (G) and AMBER (H). RNA-tomatine complex could only be simulated in CHARMM36 forcefield (see Supp. Data 2) in CHARMM-GUI, while AMBER was not

CHARMM36 berberine provides higher fluctuation of in ΔRMSD results (Figure 4B), both have a similar profile in terms of hydrogen bonds (Figure 5C and E, for berberine and colchicine, respectively). Thus both are assumed to be equally stable during simulation.

4. Discussion

The alkaloids used in this study are mostly having good drug-likeness properties, except for tomatine. The statement is based on how 4 out of 5 alkaloids obey LRo5 without a single violation, moderate bioavailability, and relatively low synthetic accessibility values. The low bioavailability index (0.17) in tomatine indicates how the alkaloid is hard to reach the systemic bloodstream and get into the designated target. The bioavailability index is ranged from 0 to 1, closer to 0 means the metabolite will hardly reach the target, while closer to 1 indicates otherwise (Shargel and Yu 2015). Bioavailability index equal to 1 refers to the metabolite or drug that is administered directly via intravenous injection (Flynn 2007), hence instantly reaching the systemic bloodstream. The synthetic accessibility value is ranged from 1 to 10, with 1 being the easiest to synthesize and 10 is the hardest, whereas tomatine hits a perfect 10 for this value. This value is determined by the complexity of a molecular structure (Ertl and Schuffenhauer 2009). By the results, the bioavailability indexes of merafloxacin (control drug), berberine, colchicine and nicotine are equally 0.55 and the synthetic accessibility values are respectively, 3.33, 3.14, 3.87 and 2.05 (as nicotine is the smallest and simplest molecule of all five). To improve the bioavailability of the compounds, drug delivery methods, e.g., lipid or chitosan nanoparticles (Cai *et al.* 2010), will be required to reach the specified RNA target. If compared to synthetic accessibility, berberine wins over colchicine.

The molecular docking scoring by AnnapuRNA and bond visualization by Discovery Studio and fingeRNAt revealed unique results. Tomatine has the highest docking score and total bonds, which is highly possible due to its large molecular structure. However, excluding tomatine and comparing to merafloxacin (control), berberine and colchicine are the top candidates. Berberine docking score is higher than merafloxacin (-157.078 kcal/mol versus -143.764 kcal/mol), but the bond is much lower than merafloxacin (9) and even colcichine (7) (but identical to nicotine, 3 bonds). Colchicine has 7 bonds, still lower than merafloxacin but higher than berberine and nicotine, but the docking score is low (-63.043 kcal/mol). Even pre-scoring (results from Autodock Vina at docking RMSD = 0 Å; the results are not used since Vina scoring is for protein-ligand docking), the docking binding affinities are -6.6 kcal/mol, -6.5 kcal/mol, -5.9 kcal/mol, -4.4 kcal/mol and -8.5 kcal/mol for merafloxacin, berberine, colchicine, nicotine and tomatine, respectively. The high docking score results in berberine are probably to the molecule tendency to intercalate between the RNA strands properly, thus creating stronger bonds in the RNA cavity. Berberine is already known as a potent metabolite for DNA intercalator and could inhibit human cytomegalovirus (HCMV) (Luganini *et al.* 2019) and herpes simplex virus (HSV) (Song *et al.* 2014). Colchicine is referred by literature to possess DNA-intercalating antiviral properties against human immunodeficiency virus type 1 (HIV-1) (Abookleesh *et al.* 2022). However, the literature appears to mistakenly see Table 2 description in the cited reference (Wink 2020), which has antiviral compounds but to quote “For DNA-intercalating alkaloids, see Table 3 (in Wink 2020)”. There is berberine referred, but unfortunately, no colchicine mentioned as one of the intercalating agents in the paper by Wink (2020). Colchicine is addressed as a DNA intercalator in older literature (Buszman *et al.* 1977). Nevertheless, further studies are required.

For molecular dynamics results in general, CHARMM36 forcefield simulation results from NAMD provided slightly superior results compared to AMBER forcefield. The graphic or RNA and RNA-alkaloid ligands in CHARMM36 appear to be less wildly fluctuating than AMBER (although the ligand in AMBER is more stable). Therefore, this study shows that simulation with CHARMM36 forcefield provides better stability for RNA-ligand interaction than AMBER. The results from this study can probably be useful for future modification and upgrade for both forcefields. In terms of results, both berberine and colchicine are equally stable throughout simulations with similar hydrogen bonds profile in CHARMM36 results. However, colchicine has more bonds in AMBER results.

In conclusion from this study, berberine (obeying LRo5, moderate bioavailability index and low synthetic accessibility value, high docking score and stable RMSD) is the most prospective as an RNA-

targeting drug. This reductionist study requires *in vitro* bioassays to improve the result data and probably optimized RNA-targeting drug delivery method to enhance the targeting method in a wide biological system. However, the methodology in this paper itself can be used for developing drugs or natural-based compound drugs. Additionally, future improvements for docking pipeline and molecular dynamics forcefield adjustment will be required to improve the accuracy of this protocol.

Acknowledgments

We are grateful to Assoc. Prof. Dr. Adolfo Rivero-Müller (Department of Biochemistry and Molecular Biology, Medical University of Lublin, Poland) for his useful insight for our research in this paper. The early concept of this paper was presented at the 5th International Symposium on Bioinformatics 2021 (InSyB2021) – Bezmialem University, Istanbul, Turkey (online) on December 15, 2021, which conference abstract has been archived in Wicaksono and Parikesit (2022).

References

Abookleesh, F.L., Al-Anzi, B.S., Ullah, A., 2022. Potential antiviral action of alkaloids. *Molecules.* 27, 903. https://doi.org/10.3390/molecules27030903

Atkins, J.F., Loughran, G., Bhatt, P.R., Firth, A.E., Baranov, P.V., 2016. Ribosomal frameshifting and transcriptional slippage: from genetic steganography and cryptography to adventitious use. *Nucleic Acids Res.* 44, 7007-7078. https://doi.org/10.1093/nar/gkw530

Baltimore, D., 1971. Expression of animal virus genomes. *Bacteriol. Rev.* 35, 235-241. https://doi.org/10.1128/br.35.3.235-241.1971

Buszman, E., Wilczok, T., Witman, B., Siebert, G., 1977. Interaction of colchicine with DNA molecules. *Hoppe Seylers Z. Physiol. Chem.* 358, 819-824. https://doi.org/10.1515/bchm2.1977.358.2.819

Cai, Z., Wang, Y., Zhu, L.-J., Liu, Z.-Q., 2010. Nanocarriers: a general strategy for enhancement of oral bioavailability of poorly absorbed or pre-systemically metabolized drugs. *Curr. Drug Metab.* 11, 197-207. https://doi.org/10.2174/138920010791110836

Cornell, W.D., Cieplak, P., Bayly, C.I., Gould, I.R., Merz, K.M., Ferguson, D.M., Spellmeyer, D.C., Fox, T., Caldwell, J.W., Kollman, P.A., 1995. A second generation force field for the simulation of proteins, nucleic acids, and organic molecules. *J. Am. Chem. Soc.* 117, 5179-5197. https://doi.org/10.1021/ja00124a002

Craigen, W.J., Caskey, C.T., 1986. Expression of peptide chain release factor 2 requires high-efficiency frameshift. *Nature.* 322, 273-275. https://doi.org/10.1038/322273a0

Daina, A., Michielin, O., Zoete, V., 2017. SwissADME: a free web tool to evaluate pharmacokinetics, drug-likeness and medicinal chemistry friendliness of small molecules. *Sci. Rep.* 7, 42717. https://doi.org/10.1038/srep42717

Ding, B., Itaya, A., 2007. Viroid: a useful model for studying the basic principles of infection and RNA biology. *Mol. Plant-Microbe Interact.* 20, 7-20. https://doi.org/10.1094/MPMI-20-0007

Dinman, J.D., 2012. Mechanisms and implications of programmed translational frameshifting. *Wiley Interdiscip. Rev. RNA.* 3, 661-673. https://doi.org/10.1002/wrna.1126

Ertl, P., Schuffenhauer, A., 2009. Estimation of synthetic accessibility score of drug-like molecules based on molecular complexity and fragment contributions. *J. Cheminformatics.* 1, 8. https://doi.org/10.1186/1758-2946-1-8

Flynn, E., 2007. Pharmacokinetic parameters, in: Enna, S.J., Bylund, D.B. (Eds.), *Pharm: The Comprehensive Pharmacology Reference*. Elsevier, New York, pp. 1-3. https://doi.org/10.1016/B978-008055232-3.60034-0

Hart, K., Foloppe, N., Baker, C.M., Denning, E.J., Nilsson, L., Mackerell, A.D., 2012. Optimization of the CHARMM additive force field for DNA: improved treatment of the BI/BII conformational equilibrium. *J. Chem. Theor. Comp.* 8, 348-362. https://doi.org/10.1021/ct200723y

Hashemian, S.M.R., Pourhanifeh, M.H., Hamblin, M.R., Shahrzad, M.K., Mirzaei, H., 2022. RdRp inhibitors and COVID-19: is molnupiravir a good option? *Biomed. Pharmacother.* 146, 112517. https://doi.org/10.1016/j.biopha.2021.112517

Humphrey, W., Dalke, A., Schulten, K., 1996. VMD: visual molecular dynamics. *J. Mol. Graph.* 14, 33-38. https://doi.org/10.1016/0263-7855(96)00018-5

Jonas, S., Izaurralde, E., 2015. Towards a molecular understanding of microRNA-mediated gene silencing. *Nat. Rev. Genet.* 16, 421-433. https://doi.org/10.1038/nrg3965

Jorgensen, W.L., Maxwell, D.S., Tirado-Rives, J., 1996. Development and testing of the OPLS all-atom force field on conformational energetics and properties of organic liquids. *J. Am. Chem. Soc.* 118, 11225-11236. https://doi.org/10.1021/ja9621760

Kelly, J.A., Olson, A.N., Neupane, K., Munshi, S., San Emeterio, J., Pollack, L., Woodside, M.T., Dinman, J.D., 2020. Structural and functional conservation of the programmed− 1 ribosomal frameshift signal of SARS coronavirus 2 (SARS-CoV-2). *J. Biol. Chem.* 295, 10741-10748. https://doi.org/10.1074/jbc.AC120.013449

Koonin, E., Gorbalenya, A., Chumakov, K., 1989. Tentative identification of RNA-dependent RNA polymerases of dsRNA viruses and their relationship to positive strand RNA viral polymerases. *FEBS Lett.* 252, 42-46. https://doi.org/10.1016/0014-5793(89)80886-5

Lee, J., Cheng, X., Swails, J.M., Yeom, M.S., Eastman, P.K., Lemkul, J.A., Wei, S., Buckner, J., Jeong, J.C., Qi, Y., Jo, S., Pande, V.S., Case, D.A., Brooks, C.L., Mackerell, A.D., Klauda, J.B., Im, W., 2016. CHARMM-GUI input generator for NAMD, GROMACS, AMBER, OpenMM, and CHARMM/OpenMM simulations using the CHARMM36 additive force field. *J. Chem. Theor. Comp.* 12, 405-413. https://doi.org/10.1021/acs.jctc.5b00935

Luganini, A., Mercorelli, B., Messa, L., Palù, G., Gribaudo, G., Loregian, A., 2019. The isoquinoline alkaloid berberine inhibits human cytomegalovirus replication by interfering with the viral Immediate Early-2 (IE2) protein transactivating activity. *Antivir. Res.* 164, 52-60. https://doi.org/10.1016/j.antiviral.2019.02.006

McNicholl, I.R., McNicholl, J.J., 2001. Neuraminidase inhibitors: zanamivir and oseltamivir. *Ann. Pharmacother.* 35, 57-70. https://doi.org/10.1345/aph.10118

Napthine, S., Ling, R., Finch, L.K., Jones, J.D., Bell, S., Brierley, I., Firth, A.E., 2017. Protein-directed ribosomal frameshifting temporally regulates gene expression. *Nat. Comm.* 8, 1-11. https://doi.org/10.1038/ncomms15582

Napthine, S., Treffers, E.E., Bell, S., Goodfellow, I., Fang, Y., Firth, A.E., Snijder, E.J., Brierley, I., 2016. A novel role for poly (C) binding proteins in programmed ribosomal frameshifting. *Nucleic Acids Res.* 44, 5491-5503. https://doi.org/10.1093/nar/gkw480

O'Boyle, N.M., Banck, M., James, C.A., Morley, C., Vandermeersch, T., Hutchison, G.R., 2011. Open babel: an open chemical toolbox. *J. Cheminformatics.* 3, 33. https://doi.org/10.1186/1758-2946-3-33

Petrov, D., Margreitter, C., Grandits, M., Oostenbrink, C., Zagrovic, B., 2013. A systematic framework for molecular dynamics simulations of protein post-translational modifications. *PLoS Comp. Biol.* 9, e1003154. https://doi.org/10.1371/journal.pcbi.1003154

Phillips, J.C., Braun, R., Wang, W., Gumbart, J., Tajkhorshid, E., Villa, E., Chipot, C., Skeel, R.D., Kalé, L., Schulten, K., 2005. Scalable molecular dynamics with NAMD. *J. Comp. Chem.* 26, 1781-1802. https://doi.org/10.1002/jcc.20289

Saxena, A., 2020. Drug targets for COVID-19 therapeutics: ongoing global efforts. *J. Biosci.* 45, 1-24. https://doi.org/10.1007/s12038-020-00067-w

Shargel, L., Yu, A.B.C., 2015. *Applied Biopharmaceutics & Pharmacokinetics,* seventh ed. McGraw-Hill, New York.

Snijder, E.J., Kikkert, M., Fang, Y., 2013. Arterivirus molecular biology and pathogenesis. *J. Gen. Virol.* 94, 2141-2163.https://doi.org/10.1099/vir.0.056341-0

Song, S., Qiu, M., Chu, Y., Chen, D., Wang, X., Su, A., Wu, Z., 2014. Downregulation of cellular c-Jun N-terminal protein kinase and NF-κB activation by berberine may result in inhibition of herpes simplex virus replication. Antimicrob. *Agents Chemother*. 58, 5068-5078. https://doi.org/10.1128/AAC.02427-14

Stage-Zimmermann, T.K., Uhlenbeck, O.C., 1998. Hammerhead ribozyme kinetics. *RNA.* 4, 875-889. https://doi.org/10.1017/S1355838298980876

Stefaniak, F., Bujnicki, J.M., 2021. AnnapuRNA: A scoring function for predicting RNA-small molecule binding poses. *PLoS Comp. Biol.* 17, e1008309. https://doi.org/10.1371/journal.pcbi.1008309

Sun, Y., Abriola, L., Niederer, R.O., Pedersen, S.F., Alfajaro, M.M., Silva Monteiro, V., Wilen, C.B., Ho, Y.-C., Gilbert, W.V., Surovtseva, Y.V., 2021. Restriction of SARS-CoV-2 replication by targeting programmed− 1 ribosomal frameshifting. *Proc. Natl. Acad. Sci.* 118, e2023051118. https://doi.org/10.1073/pnas.2023051118

Szulc, N.A., Mackiewicz, Z., Bujnicki, J.M., Stefaniak, F., 2022. fingeRNAt-A novel tool for high-throughput analysis of nucleic acid-ligand interactions. *PLoS Comp. Biol.* 18, e1009783. https://doi.org/10.1371/journal.pcbi.1009783

Trott, O., Olson, A.J., 2009. AutoDock Vina: Improving the speed and accuracy of docking with a new scoring function, efficient optimization, and multithreading. *J. Comp. Chem.* 31, 455-461. https://doi.org/10.1002/jcc.21334

Wicaksono, A., Parikesit, A.A., 2022. Plant Alkaloid Potential Antiviral Intercalating Drug Screening Through RNA-Ligand Molecular Docking Methods: Early Test on SARS-CoV-2 RNA Fragment. 5th International Symposium on Bioinformatics (InSyB2021), 21.

Wink, M., 2020. Potential of DNA intercalating alkaloids and other plant secondary metabolites against SARS-CoV-2 causing COVID-19. *Diversity*. 12, 175. https://doi.org/10.3390/d12050175

Xu, Y., Vanommeslaeghe, K., Aleksandrov, A., Mackerell, A.D., Nilsson, L., 2016. Additive CHARMM force field for naturally occurring modified ribonucleotides. *J. Comp. Chem.* 37, 896-912. https://doi.org/10.1002/jcc.24307

Zgarbová, M., Otyepka, M., Šponer, J., Mládek, A., Banáš, P., Cheatham, T.E., Jurečka, P., 2011. Refinement of the cornell et al. nucleic acids force field based on reference quantum chemical calculations of glycosidic torsion profiles. *J. Chem. Theor. Comp.* 7, 2886-2902. https://doi.org/10.1021/ct200162x

Zhang, K., Zheludev, I.N., Hagey, R.J., Haslecker, R., Hou, Y.J., Kretsch, R., Pintilie, G.D., Rangan, R., Kladwang, W., Li, S., 2021. Cryo-EM and antisense targeting of the 28-kDa frameshift stimulation element from the SARS-CoV-2 RNA genome. *Nat. Struct. Mol. Biol.* 28, 747-754. https://doi.org/10.1038/s41594-021-00653-y

Zhang, L., Zhou, R., 2020. Structural basis of the potential binding mechanism of remdesivir to SARS-CoV-2 RNA-dependent RNA polymerase. *J. Phys. Chem. B.* 124, 6955-6962. https://doi.org/10.1021/acs.jpcb.0c04198